
Towards a Unified Framework of Contrastive Learning for Disentangled Representations

Stefan Matthes, Zhiwei Han, Hao Shen
fortiss GmbH, Munich, Germany
{matthes,han,shen}@fortiss.org

Abstract

Contrastive learning has recently emerged as a promising approach for learning data representations that discover and disentangle the explanatory factors of the data. Previous analyses of such approaches have largely focused on individual contrastive losses, such as noise-contrastive estimation (NCE) and InfoNCE, and rely on specific assumptions about the data generating process. This paper extends the theoretical guarantees for disentanglement to a broader family of contrastive methods, while also relaxing the assumptions about the data distribution. Specifically, we prove identifiability of the true latents for four contrastive losses studied in this paper, without imposing common independence assumptions. The theoretical findings are validated on several benchmark datasets. Finally, practical limitations of these methods are also investigated.

1 Introduction

Learning to disentangle the explanatory factors of the observed data is valuable for a variety of machine learning (ML) applications, as it allows for a more compact, interpretable, and manipulable data representation. Consequently, this can improve sampling efficiency [54] and predictive performance [41, 13, 15] for downstream tasks, and promote fairness [39, 10]. Among the many efforts to develop a theoretically grounded approach to learning such representations, contrastive learning (CL) has emerged as a particularly promising technique.

Intuitively, contrastive methods learn a function that maps observations into a representation space, such that related examples (e.g., augmentations of the same sample) are mapped close to each other and negative pairs are mapped far apart [8, 56]. In recent years, this intuition has been refined and extended by different theories. One of these theories is that contrastive methods (approximately) invert the data generating process [58, 28] and thus recover the generative factors. We build upon this line of work and extend their theoretical findings to a wider range of contrastive objectives.

In this study, we aim to develop a unified framework of statistical priors on the data generating process to improve our understanding of CL for disentangled representations. Two important issues we will discuss are how to deal with nonuniform marginal distributions of the latent factors and situations when these factors are conditionally dependent to some degree. We demonstrate how this could be accomplished with a simple modification of common contrastive objectives. We also show that without these modifications, contrastive objectives make implicit assumptions about the data generating process and investigate when these assumptions are justified. We empirically verify our theoretical claims and show practical limitations of the proposed framework.

In short, the contributions of our study can be summarized as follows:

- We extend and unify theoretical guarantees of disentanglement for a family of contrastive losses under relaxed assumptions about the data generating process.

- The theoretical findings are empirically validated on several benchmark datasets and we quantitatively compare the disentanglement performance of four contrastive losses.
- We analyze the impact of partially violated assumptions and investigate practical limitations of the proposed framework.

2 Related Work

Disentangled Representation Learning The concept of learning representations whose components correspond to the explanatory factors of the data can be traced back to the principles of blind source separation [7] and discovering factorial codes [3]. In contrast to earlier work, however, the research focus has gradually shifted to applications where the relationship between data and underlying factors is nonlinear.

The difficulty of this task is that for independent and identically distributed (i.i.d.) data that depend nonlinearly on the latent factors, it is fundamentally impossible to identify these factors without labels or assumptions about the data generating process [27, 40, 30].

A few studies showed how the underlying generative factors can be recovered if they are mutually independent (with at most one of them being Gaussian) and their relation to the observed data exhibits certain regularities, such as a linear mixture followed by an element-wise nonlinearity [50], and local isometries [24]. Gresele et al. [17] also showed that conformal maps rule out some spurious solutions.

Most approaches, however, depart from the i.i.d. assumption and utilize co-observed dependent variables, such as a time index [25] or prior observations [26] in a time-series, observations obtained from interventions [42], data augmentation [55] or different views [16]. These approaches mainly differ in how they model the statistical and causal dependencies between the latent factors and their relation to the auxiliary variable.

Hyvärinen et al. [28] modeled the distribution of the latent factors with the exponential family, where the key assumptions are that, for a given auxiliary variable, the latent factors are conditionally independent and that the effect of the auxiliary variable on their distributions is sufficiently diverse. Their theory was later extended to the Variational Autoencoder (VAE [33]) framework [30] and to energy-based models [31] with further relaxed independence assumptions. Other conditional distributions that have been considered are the Laplace distribution [34] and the von Mises–Fisher distribution [58]. In this work, we extend these results to distance-based conditional distributions and arbitrary marginals of the latents.

Another research direction considers pairs of observations whose underlying latents differ only in some of the factors and share the others, for example, through interventions or actions. In [49, 38] the shared factors or intervention targets are assumed to be known. Locatello et al. [42] showed how the ground-truth latents can be recovered when the pairs of observations share at least one latent factor, which was extended to multi-dimensional factors in [12], but their approaches additionally require that the latent factors are mutually independent. In contrast, [35, 1, 5] proved identifiability for more general causal dependencies between the latent factors by exploiting sparse transitions.

Contrastive Learning In recent years, contrastive methods have shown a remarkable ability to learn useful representations for downstream tasks [45, 47, 8, 21, 20]. A number of works attribute this success primarily to their tendency to maximize mutual information (MI) between latent representations [47, 23, 2, 51]. However, it has been observed that contrastive objectives with tighter MI bounds do not necessarily enhance downstream performance [53, 52].

More recently, by exploiting the alignment and uniformity properties [56] of InfoNCE [47], Zimmermann et al. [58] showed that InfoNCE approximately inverts the data generating process, leading to the identification of the true latent factors. We extend this theory to a broader family of contrastive methods [47, 18, 20, 46].

3 Contrastive Learning for Disentangled Representations

In this section, we present our theoretical framework of contrastive methods for learning disentangled representations (Figure 1). We begin with the formalization of our assumptions on the underlying data generating process.

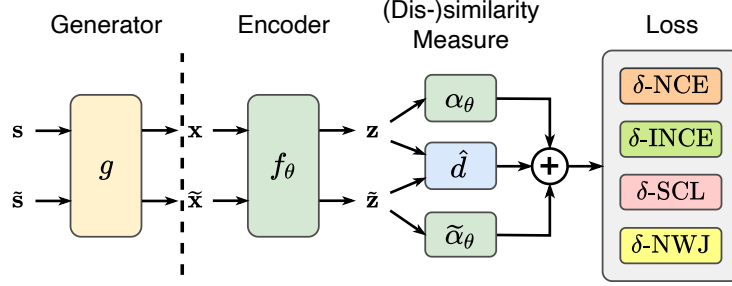


Figure 1: Overview of our CL framework for disentanglement. The unknown generator g maps latent pairs $(s, \tilde{s}) \sim p(s, \tilde{s})$ to observation pairs (x, \tilde{x}) , which are encoded by f_θ . After computing the dissimilarity measure according to Eq. (2), the representation is optimized with one of the contrastive losses.

3.1 Data Generating Process

In this work, we adopt the common assumption that the observations are generated by a smooth and invertible generator $g: \mathcal{S} \rightarrow \mathcal{X}$, where $\mathcal{S} \subseteq \mathbb{R}^n$ denotes the space of latent factors and $\mathcal{X} \subseteq \mathbb{R}^m$ the space of observations. Here, we assume $n \leq m$. The goal is to find a function $f: \mathcal{X} \rightarrow \mathcal{Z} \subseteq \mathbb{R}^n$ that inverts g up to element-wise transformations or other simple mappings such as linear functions.

We do not impose any constraints on the ground-truth marginal distribution of the latents, $p(s)$, except that the support must be connected. Let $s \sim p(s)$ and (s, \tilde{s}) be a latent positive pair. We model the dependency between s and \tilde{s} with the following conditional distribution

$$p(\tilde{s}|s) = \frac{Q(\tilde{s})}{Z(s)} e^{-d(s, \tilde{s})} \quad \text{with} \quad Z(s) = \int_{\mathcal{S}} Q(\tilde{s}) e^{-d(s, \tilde{s})} d\tilde{s}, \quad (1)$$

where Q and Z are scalar-valued functions and d is a distance function, which we will specify below. It is worth noticing that here the latent factors s_i are not assumed to be statistically independent or conditionally independent given auxiliary observations (Q cannot necessarily be factorized).

Two related observations (e.g., consecutive frames in a sequence, multiple views or augmentations of the same data point) are then generated by $x = g(s)$ and $\tilde{x} = g(\tilde{s})$. For the sake of simplicity, we assume that the related instances are of the same modality, though it is straightforward to extend this framework to different modalities, such as image and audio coming from different generators.

3.2 Contrastive Learning Approaches

Contrastive methods generally have in common that they employ certain mechanisms to measure similarity between data points. The most frequent choice is the cosine similarity [8], while ℓ_p distances [9, 58] and even learnable functions [26, 28] have also been used. Inspired by the work in [26, 28], which relies on specific models of learnable similarity measures, we propose the following generic dissimilarity measure

$$\delta(z, \tilde{z}) = \hat{d}(z, \tilde{z}) + \alpha(z) + \tilde{\alpha}(\tilde{z}), \quad (2)$$

where α and $\tilde{\alpha}$ are learnable scalar-valued functions, e.g., neural networks, and \hat{d} is a fixed expression that describes the interaction between related examples. In the ideal case, \hat{d} matches d in Eq. (1).

Let us now recall some common contrastive methods. The first approach we investigate is noise-contrastive estimation (NCE) [18], which has been used for disentanglement in [26, 28]. Using our dissimilarity measure, the loss can be formulated as follows

$$\mathcal{L}_{\delta\text{-NCE}}(f, \delta) = \mathbb{E}_{(x, \tilde{x}) \sim p_{\text{pos}}} -\log[\text{sig}(-\delta(f(x), f(\tilde{x})))] - \mathbb{E}_{x, x' \sim p} \log[1 - \text{sig}(-\delta(f(x), f(x')))], \quad (3)$$

where sig is the sigmoid function, p_{pos} is the distribution of positive pairs, and p is the distribution of all observations.¹

¹For simplicity, we assume here that both marginal distributions are the same. We consider the more general case of different marginals in the supplementary material.

Another popular choice is InfoNCE, which has shown remarkable success in self-supervised learning [47, 8, 23, 21]. The loss function has several related forms and has been referred to by different names [29, 47, 8, 36]. In the following, we use

$$\mathcal{L}_{\delta\text{-INCE}}(f, \delta; K) = \mathbb{E}_{\substack{(\mathbf{x}, \tilde{\mathbf{x}}) \sim p_{\text{pos}} \\ \{\mathbf{x}_i^-\}_{i=1}^K \stackrel{\text{i.i.d.}}{\sim} p}} - \log \frac{e^{-\delta(f(\mathbf{x}), f(\tilde{\mathbf{x}}))}}{e^{-\delta(f(\mathbf{x}), f(\tilde{\mathbf{x}}))} + \sum_{i=1}^K e^{-\delta(f(\mathbf{x}), f(\mathbf{x}_i^-))}}, \quad (4)$$

where $K \geq 1$ is the number of negative examples. Since $\mathcal{L}_{\delta\text{-INCE}}$ is invariant to changes in α , we simply set $\alpha(\mathbf{z}) = 0$ in this case.

HaoChen et al. [20] introduced the concept of spectral contrastive learning (SCL), which has classification guarantees for downstream tasks in the context of self-supervised learning. To fit this method into our theoretical framework, we use a slightly modified version in our analysis, where we substitute $f(\mathbf{x})^\top f(\tilde{\mathbf{x}})$ with $e^{-\delta(f(\mathbf{x}), f(\tilde{\mathbf{x}}))}$, i.e.,

$$\mathcal{L}_{\delta\text{-SCL}}(f, \delta) = \mathbb{E}_{(\mathbf{x}, \tilde{\mathbf{x}}) \sim p_{\text{pos}}} -2 e^{-\delta(f(\mathbf{x}), f(\tilde{\mathbf{x}}))} + \mathbb{E}_{\mathbf{x}, \mathbf{x}^- \sim p} e^{-2\delta(f(\mathbf{x}), f(\mathbf{x}^-))}. \quad (5)$$

Finally, we examine the Nguyen-Wainwright-Jordan (NWJ) objective [46] using the same dissimilarity measure as before

$$\mathcal{L}_{\delta\text{-NWJ}}(f, \delta) = \mathbb{E}_{(\mathbf{x}, \tilde{\mathbf{x}}) \sim p_{\text{pos}}} \delta(f(\mathbf{x}), f(\tilde{\mathbf{x}})) + \mathbb{E}_{\mathbf{x}, \mathbf{x}^- \sim p} e^{-\delta(f(\mathbf{x}), f(\mathbf{x}^-))}. \quad (6)$$

Note, that we here use it as a loss instead of a lower bound on MI. To the best of our knowledge, neither the SCL nor the NWJ objective have been employed to learn disentangled representations or for ICA.

3.3 Identifiability

In this section, we derive precise conditions on the data generating process under which the relationship between the learned representation and true latent factors can be described by a simple function. In line with [31], we speak of weak identifiability when this function is an affine mapping, and of strong identifiability when it is a generalized permutation matrix.²

As in previous research [34, 58], we assume that the interaction between \mathbf{s} and $\tilde{\mathbf{s}}$ is (approximately) known, i.e., \hat{d} in the dissimilarity measure as defined in Eq. (2) matches d in the conditional distribution defined in Eq. (1). Although this is a strong restriction on the latent factors, satisfactory performance is still observed in practice, even when the assumption is violated. Note also that if they only match up to other simple transformations (e.g., invertible element-wise) of the true or learned latents, the recovered relation can be extended by just those transformations.

First, we study the case of weak identifiability. Eq. (1) essentially states that the joint probability density function of positive pairs decreases exponentially with the distance between the underlying latent factors, distorted only by $Q(\tilde{\mathbf{s}})$ and the marginal distribution $p(\mathbf{s})$. Neither $Q(\tilde{\mathbf{s}})$ nor $p(\mathbf{s})$ depends on both instances of a pair. This allows us to learn a distance-preserving representation while accumulating factors that depend exclusively on the first or second element in α and $\tilde{\alpha}$, respectively. We formalize this in the following theorem.

Theorem 1 (Weak identifiability). *Let $\mathcal{S} \subseteq \mathbb{R}^n$ be open and connected, $\mathcal{X} \subseteq \mathbb{R}^m$, and $g: \mathcal{S} \rightarrow \mathcal{X}$ invertible and differentiable. Let us further assume that the observed data satisfy the generative model given in Eq. (1). If $d = \hat{d}$ has one of the following properties:*

- (i) *there exists a function $\xi: \mathbb{R}^+ \rightarrow \mathbb{R}^+$, such that $\xi \circ d$ is a norm-induced metric³,*
- (ii) *$d(\mathbf{s}, \tilde{\mathbf{s}}) = \sum_i d_i(|s_i - \tilde{s}_i|)$, where each d_i is continuous and strictly increasing,*

then the optimal estimator of any of the contrastive losses presented above identifies the true latent factors up to affine transformations, i.e., $h = f \circ g$ is an affine mapping.

²This property is sometimes called explicitness [48] or informativeness [11], when it is left open what is meant by a simple function.

³A norm-induced metric is a metric which is translation invariant, $d(\mathbf{x}, \mathbf{y}) = d(\mathbf{x} + \mathbf{b}, \mathbf{y} + \mathbf{b})$, and absolutely homogeneous, $d(\sigma\mathbf{x}, \sigma\mathbf{y}) = |\sigma|d(\mathbf{x}, \mathbf{y})$

The central idea of the proof, which can be found in the supplementary material, is to show that the learned representation preserves the distance from the latent space, i.e., $d(\mathbf{s}, \tilde{\mathbf{s}}) = d(h(\mathbf{s}), h(\tilde{\mathbf{s}}))$. Further, by constraining the dimension and connectivity of the latent space, such a mapping must be affine. As a byproduct of the derivation, we obtain for the global optimum that

$$\tilde{\alpha} \circ h = \log p - \log Q \quad (7)$$

and, except for $\mathcal{L}_{\delta\text{-INCE}}(f, \delta; K)$,

$$\alpha \circ h = \log Z. \quad (8)$$

We verify this with a simple example in Figure 2. This means that when we optimise the InfoNCE objective with $\tilde{\alpha}$ set to zero, we implicitly assume that $Q = p$. This is true, for example, when the marginal distribution is uniform and Q is constant. Thus, our theorem is consistent with the perspective of uniformity and alignment [56] and can be seen as a generalization of Theorem 5 from [58]. In particular, we extend their results to other contrastive losses, nonconvex latent spaces, nonuniform marginal distributions, and even to the case where the latent factors are not conditionally independent.

Next we show strong identifiability when d in the conditional distribution of the latent factors is further restricted. The proof can be found in the supplementary material.

Theorem 2 (Strong identifiability). *Assume that all conditions in Theorem 1 are satisfied. Let the function d from Eq. (1) be defined by*

$$d(\mathbf{s}, \tilde{\mathbf{s}}) = \sum_i (|s_i - \tilde{s}_i|/\sigma_i)^\beta, \quad (9)$$

with $\beta \in (0, 2) \cup (2, \infty)$ and $\sigma_i > 0$ for all i , then $h = f \circ g$ is a generalized permutation matrix, i.e., a composition of a permutation and element-wise scaling and sign flips.

This result is similar to earlier theorems [34, 58], but relaxes some conditions. In particular, it also holds for nonuniform marginals and $\beta \in (0, 1)$. For the case $\beta = 2$, the conditional distribution is quasi-Gaussian [26] and, as with linear Independent Component Analysis (ICA) for normally distributed sources, strong identifiability is then provably impossible.

In contrast to [28], we show identifiability for the generalized normal distribution (excluding $\beta = 2$) and do not assume some regularity conditions, e.g., that the encoder is twice differentiable and invertible. However, we do not claim to generalize their results, since the exponential family contains distributions that we do not consider here.

Theorem 2 also has an interesting connection to some recently proposed disentanglement methods that rely on sparsity [35, 1]. This situation is similar to the case when $\beta \rightarrow 0$ in Eq. (9) and the conditional $p(\tilde{\mathbf{s}}|\mathbf{s})$ becomes sparse. However, this is a topic for future work.

4 Experiments

In this section, we conduct a comprehensive quantitative evaluation of our theoretical framework. We largely adopt the experimental setup and evaluation protocol of [58] with one major difference. During training, we additionally optimize for α and $\tilde{\alpha}$ in Eq. (2), both of which are parameterized by three-layer neural networks, respectively. In practice, both functions are normalized to a mean of zero and are jointly trained with a learnable offset c , i.e., $\delta(\mathbf{z}, \tilde{\mathbf{z}}) = \hat{d}(\mathbf{z}, \tilde{\mathbf{z}}) + \alpha(\mathbf{z}) + \tilde{\alpha}(\tilde{\mathbf{z}}) + c$. In the case of δ -INCE, we use $\delta(\mathbf{z}, \tilde{\mathbf{z}}) = \hat{d}(\mathbf{z}, \tilde{\mathbf{z}}) + \tilde{\alpha}(\tilde{\mathbf{z}})$ instead. Further details on the implementation can be found in the supplementary material.

As in previous research [25, 26, 58], we test for weak identifiability, i.e., up to affine transformations, by fitting a linear regression model between the ground-truth and recovered latents and compute the coefficient of determination (R^2). For strong identifiability, i.e., up to generalized permutations and element-wise transformations, we report the mean correlation coefficient (MCC).

4.1 Validation of Theoretical Findings

To validate our theoretical claims, we adopt a generative process similar to [58]. However, to demonstrate that identifiability can be achieved for nonconvex latent spaces, nonuniform marginals,

Table 1: Identifiability on synthetic data. MCC [%] mean \pm standard deviation over 2 random seeds

Scenario	β	δ -NCE	δ -INCE	δ -SCL	δ -NWJ
Box (simple)	1/2	99.68 \pm 0.04	99.56 \pm 0.18	87.08 \pm 1.40	99.80 \pm 0.02
Box (simple)	1	99.91 \pm 0.01	99.90 \pm 0.01	94.33 \pm 2.02	99.87 \pm 0.01
Box (simple)	3	99.66 \pm 0.20	96.97 \pm 2.47	98.29 \pm 0.14	99.71 \pm 0.05
Box (simple)	5	99.79 \pm 0.02	96.56 \pm 2.44	98.63 \pm 0.36	99.74 \pm 0.00
Box (complex)	1	99.13 \pm 0.41	99.87 \pm 0.05	83.73 \pm 2.49	93.14 \pm 4.97
Box (complex)	3	99.90 \pm 0.00	99.84 \pm 0.00	93.64 \pm 0.22	99.84 \pm 0.00
Hollow ball	1	99.73 \pm 0.11	99.70 \pm 0.08	90.27 \pm 6.48	99.73 \pm 0.08
Hollow ball	3	95.82 \pm 4.65	98.05 \pm 0.08	97.65 \pm 0.00	99.03 \pm 0.06
Hollow ball	5	98.52 \pm 0.21	96.25 \pm 0.43	97.57 \pm 0.06	98.67 \pm 0.16
Cube grid	1	99.87 \pm 0.02	99.66 \pm 0.04	96.92 \pm 1.88	99.79 \pm 0.01
Cube grid	5	97.42 \pm 0.12	82.26 \pm 7.06	96.17 \pm 0.07	97.96 \pm 0.06

and without conditionally independent latents, we investigate additional configurations of these components.

In this section, we consider latent spaces with $n = 10$ dimensions. We generate pairs of source signals $(\mathbf{s}, \tilde{\mathbf{s}})$ by first sampling from a marginal distribution $p(\mathbf{s})$ and subsequently from a conditional distribution

$$p(\tilde{\mathbf{s}}|\mathbf{s}) = \frac{Q(\tilde{\mathbf{s}})}{Z(\mathbf{s})} e^{-\sum_i \left(\frac{|s_i - \tilde{s}_i|}{\sigma}\right)^\beta}. \quad (10)$$

The observations $(\mathbf{x}, \tilde{\mathbf{x}})$ are then generated by passing \mathbf{s} and $\tilde{\mathbf{s}}$ individually through an (approximately) invertible multilayer perceptron (MLP).

We analyze the following four scenarios where we vary \mathcal{S} , $p(\mathbf{s})$, Q and β :

- Box (simple): $\mathcal{S} = [0, 1]^n$, $p(\mathbf{s})$ is uniform, Q is constant. This is our baseline.
- Box (complex): $\mathcal{S} = [0, 1]^n$, $p(\mathbf{s})$ is a normal distribution with block-diagonal correlation matrix such that the odd dimensions are correlated with the even dimensions, Q has a checkerboard pattern (i.e., has value 1 on “white squares” and 0.1 on “black squares”), so the latent factors are not conditionally independent.
- Hollow ball: $\mathcal{S} = \{\mathbf{s} \in \mathbb{R}^n \mid r < \|\mathbf{s}\| < R, 0 < r < R\}$ with inner radius r and outer radius R , $p(\mathbf{s})$ is uniform over the radius and angle (but not uniform in Euclidean coordinates), Q is constant. Note that here \tilde{s}_i and \tilde{s}_j are not conditionally independent given \mathbf{s} , because the support is not rectangular.
- Cube grid: $\mathcal{S} = \{\mathbf{s} \in [-1, 1]^n \mid \forall i : s_i < -b \vee s_i > b, 0 < b < 1\}$ (i.e., \mathcal{S} is disconnected), $p(\mathbf{s})$ is uniform, Q is constant. Although our current analysis makes no predictions about disconnected spaces, we investigate this configuration to empirically probe potential limits of our framework.

To fit our hardware setup, we use a smaller batch size of 5120. Also, we use an encoder network with residual connections and batch normalization, which has been shown to be more stable. We generally leave the output space unrestricted, i.e., $\mathcal{Z} = \mathbb{R}^n$.

Table 1 provides a summary of the MCC scores. The corresponding R^2 values can be found in the supplementary material. In each scenario, all contrastive losses achieve near-optimal disentanglement, with the exception of a few outliers. In particular, δ -SCL appears to be numerically less stable than its counterparts, which we will examine in more detail in later sections. Additional experiments in the supplementary material compare δ -SCL with the original SCL and show that δ -SCL generally yields higher disentanglement scores. However, we would like to point out that one should not draw direct conclusions from these results about the performance of the original SCL on other downstream tasks.

To verify that the learned functions $\tilde{\alpha}$ and α converge to the solution given in Eq. (7) and Eq. (8), we construct a simple example where the ground truth is known. We choose $\mathcal{S} = \mathcal{Z} = [0, 1]^2$ with a uniform marginal distribution. The positive examples are sampled from a truncated Laplace

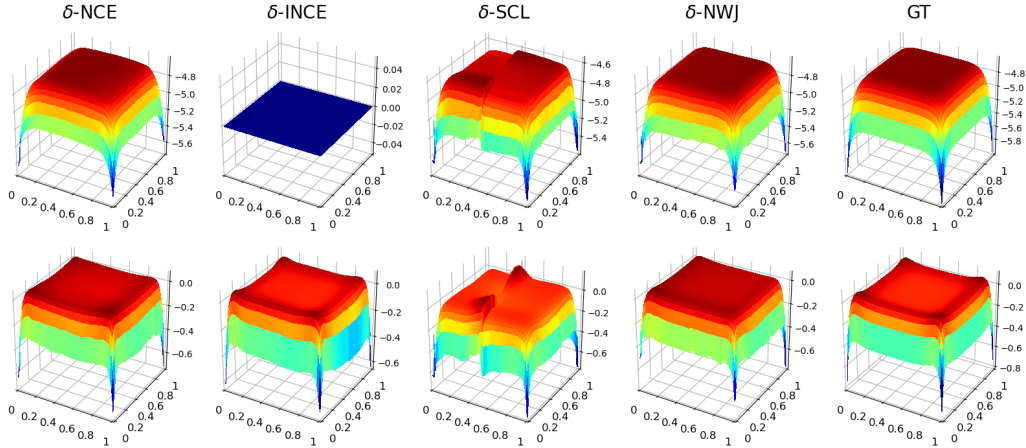


Figure 2: Learned functions α (top row) and $\tilde{\alpha}$ (bottom row) for a simple example described in the text. The ground truth is in the right column. In the case of δ -INCE, α is set to zero.

Table 2: MCC [%] scores on synthetic data for $\alpha(\mathbf{z}) = \tilde{\alpha}(\tilde{\mathbf{z}}) = c$

Scenario	β	δ -NCE	δ -INCE	δ -SCL	δ -NWJ
Box (simple)	1/2	99.57	99.81	82.69	89.22
Box (simple)	1	99.85	99.91	94.00	99.81
Box (simple)	3	99.77	99.40	99.78	99.76
Box (simple)	5	99.82	98.86	94.84	99.82
Box (complex)	1	99.70	99.82	76.63	99.68
Box (complex)	3	99.69	99.75	89.78	99.51
Hollow ball	1	98.49	99.37	87.31	97.94
Hollow ball	3	98.59	97.23	96.39	98.64
Hollow ball	5	98.52	96.26	98.49	98.52
Cube grid	1	99.82	99.39	98.21	99.75
Cube grid	5	96.53	84.73	97.50	97.42

distribution. Figure 2 shows the results. Details and additional experimental setups can be found in the supplementary material.

Since we learn the sum of α and $\tilde{\alpha}$, they can only be identified up to some offset. In Figure 2, we have added the learned bias to α to confirm that the total offset is correct. All losses reach the global optimum except for δ -SCL, which appears to be stuck at a local minimum.

4.2 Evaluation under Partially Violated Assumptions

We also report results for the case where α and $\tilde{\alpha}$ are set to a learnable constant (see Table 2). Interestingly, we do not observe that this change significantly affects the outcome. However, we do observe a drastic performance drop in δ -NCE, δ -SCL and δ -NWJ when this offset is fixed to a value which is far from the ground truth. Specifically, setting the bias to zero causes a drop in the MCC score by more than 20% on average when $\beta = 1$. For larger β we do not observe different behaviour. This is likely due to the fact that the optimal bias is far from 0 when β is smaller, which can distort the learned representation.

4.3 Evaluation on Kitti Masks

The KITTI Masks dataset [34] consists of segmentation masks of pedestrians extracted from the autonomous driving benchmark KITTI-MOTS [14]. We compare the presented loss functions with

Table 3: KITTI Masks. MCC [%] mean \pm standard deviation over 10 random seeds

$\overline{\Delta t}$	Loss	Laplace		Normal	
		Unbounded	Box	Unbounded	Box
0.05s	SlowVAE [34]	66.1 \pm 4.5			
- " -	δ -contr [58]	77.1 \pm 1.0	74.1 \pm 4.4	58.3 \pm 5.4	59.9 \pm 5.5
- " -	δ -INCE	77.3 \pm 1.5	75.9 \pm 1.7	68.1 \pm 5.0	68.3 \pm 4.8
- " -	δ -NCE	77.1 \pm 1.0	75.4 \pm 2.4	60.2 \pm 4.9	68.0 \pm 1.5
- " -	δ -SCL	75.8 \pm 3.9	71.5 \pm 7.5	66.2 \pm 10.7	66.5 \pm 4.0
- " -	δ -NWJ	77.3 \pm 0.7	77.7 \pm 0.9	67.5 \pm 5.3	69.2 \pm 5.3
0.15s	SlowVAE [34]	79.6 \pm 5.8			
- " -	δ -contr [58]	79.4 \pm 1.9	80.9 \pm 3.8	60.2 \pm 8.7	68.4 \pm 6.7
- " -	δ -INCE	80.5 \pm 1.4	77.0 \pm 3.3	68.9 \pm 5.2	68.4 \pm 4.2
- " -	δ -NCE	79.3 \pm 2.3	79.5 \pm 2.7	62.7 \pm 4.6	68.4 \pm 3.5
- " -	δ -SCL	72.9 \pm 3.9	74.4 \pm 2.6	62.5 \pm 5.0	66.1 \pm 5.7
- " -	δ -NWJ	79.3 \pm 2.0	78.2 \pm 6.1	68.2 \pm 3.5	72.6 \pm 6.7

Table 4: 3DIdent. R^2 [%] and MCC [%] mean \pm standard deviation over 2 random seeds

β	Loss	R^2		MCC	
		Unbounded	Box	Unbounded	Box
2	δ -contr [58]	96.43 \pm 0.03	96.73 \pm 0.10	54.94 \pm 0.02	98.31 \pm 0.04
2	δ -INCE	97.87 \pm 0.07	98.08 \pm 0.03	56.09 \pm 0.10	98.98 \pm 0.09
2	δ -NCE	98.05 \pm 0.04	97.91 \pm 0.02	55.34 \pm 0.11	98.95 \pm 0.08
2	δ -SCL	71.07 \pm 3.76	74.92 \pm 2.28	49.88 \pm 1.20	76.02 \pm 3.13
2	δ -NWJ	94.03 \pm 1.35	97.67 \pm 0.02	53.82 \pm 0.46	98.79 \pm 0.02
1	δ -contr [58]		96.87 \pm 0.08		98.38 \pm 0.03
1	δ -INCE	98.03 \pm 0.06	97.45 \pm 0.04	55.79 \pm 0.09	98.63 \pm 0.05
1	δ -NCE	97.83 \pm 0.04	97.33 \pm 0.03	56.35 \pm 0.08	98.71 \pm 0.02
1	δ -SCL	78.59 \pm 3.92	93.13 \pm 1.83	52.28 \pm 1.98	95.77 \pm 2.58
1	δ -NWJ	94.02 \pm 1.28	97.64 \pm 0.09	54.87 \pm 0.33	98.82 \pm 0.03

the current state of the art for this dataset [34, 58]. Except for the additional parameters in δ , we use the same settings and follow their evaluation protocol.

As noted by Klindt et al. [34], the transitions of the latents are mostly sparse. It is therefore not surprising that all contrastive losses consistently perform better when a Laplace conditional is assumed as opposed to a normal conditional. Considering the large variance across different random seeds, all contrastive losses perform similarly well, with the largest outlier being δ -SCL, which could already be observed on the synthetic dataset in the previous section.

Overall, there are only small differences between the different embedding spaces, with about half of the methods performing better on each setup. Consistent with previous observations [58], we see for all models slightly better performance for larger time intervals, $\overline{\Delta t}$, between consecutive frames. One possible reason is that a larger concentration of the conditional leads to a larger range of δ values, causing numerical instability. We investigate this phenomenon in more detail in Section 4.5.

4.4 Evaluation on 3DIdent

We additionally evaluate our framework under partially violated assumptions on 3DIdent [58], a recently proposed benchmark dataset. The dataset is composed of rendered images showing a complex object in different positions, rotations and under different lighting conditions. Positive pairs $(\mathbf{s}, \tilde{\mathbf{s}})$ are obtained by randomly selecting \mathbf{s} and matching sampled $\tilde{\mathbf{s}}'$ from the conditional $p(\tilde{\mathbf{s}}'|\mathbf{s})$ to the closest $\tilde{\mathbf{s}}$ with a rendered image. We consider a normal ($\beta = 2$) and a Laplace conditional ($\beta = 1$). In both cases we set $\hat{d}(\mathbf{z}, \tilde{\mathbf{z}}) = \|\mathbf{z} - \tilde{\mathbf{z}}\|_2^2$ where we either leave the output space unbounded

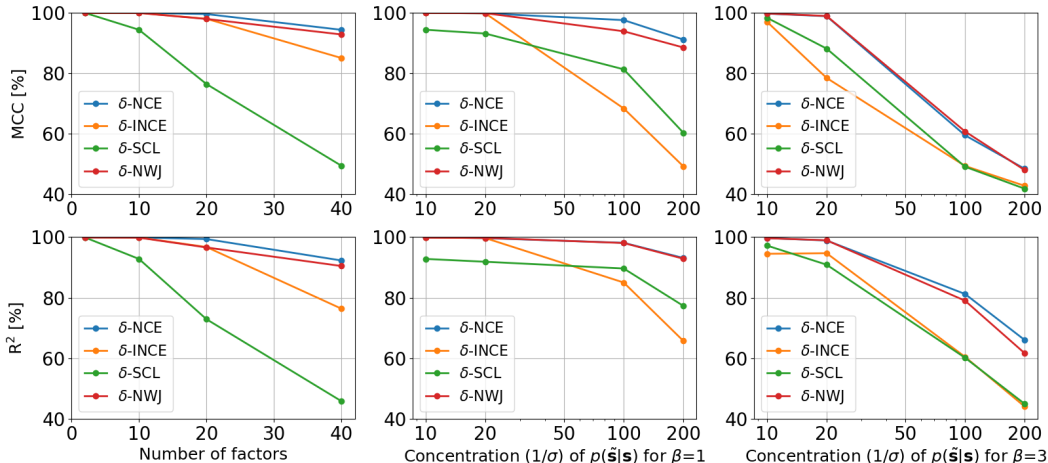


Figure 3: MCC (top) and R^2 scores (bottom) for different numbers of latent factors (left) and for different concentrations ($1/\sigma$) of the conditional distribution for $\beta = 1$ (center) and $\beta = 3$ (right).

($\mathcal{Z} = \mathbb{R}^n$) or restrict it to an adjustable box ($\mathcal{Z} = [0, b]^n$, where b is a learnable parameter). The latter is achieved by applying a sigmoid function in the last layer of the network and multiplying the result by b . Table 4 shows the results for weak and strong identifiability.

With the exception of δ -SCL, the examined contrastive losses have R^2 values close to the theoretical optimum. However, δ -NWJ shows less robustness when we do not restrict the latent space compared to δ -NCE and δ -INCE. This demonstrates that incorporating knowledge about the latent space can stabilize training and lead to strong identifiability, even in the case of a (truncated) Gaussian conditional distribution.

4.5 Investigation of Limitations

In this section, we discuss practical and theoretical limitations of the proposed framework. We first examine how changes in the number of latent factors and the concentration of the conditional distribution affect disentanglement. We use the same setup as in Section 4.1, except that we choose a slightly smaller batch size of 4096 and train for 8×10^5 iterations to ensure convergence when we consider more dimensions. The results are shown in Figure 3.

First, we note that all methods have difficulties when the number of latent factors is increased (see Figure 3, left column). In particular, δ -SCL shows little robustness for larger dimensions.

Furthermore, we see that the performance of all methods declines with increasing concentration ($1/\sigma$) of the conditional and is exacerbated by a larger shape parameter (β). The work in [58] noted that InfoNCE has difficulty disentangling the latent factors when the conditional distribution becomes too flat relative to the marginal one, which, they pointed out, makes positive examples indistinguishable from negative ones. We observe here the same problem in the opposite case.

Consider the following example. Suppose $\mathcal{S} = [0, 1]^n$ and $p(\mathbf{s})$ is uniform, then the range of δ at the global optimum is $[0, n/\sigma^\beta]$. For larger β and smaller σ , this quickly leads to vanishing values when calculating the exponential in the contrastive losses. This could also be one of the reasons why we see worse performance for smaller Δt in KITTI Masks.

It should be noted that employing learnable functions in the similarity measure may entail certain drawbacks, such as the need to store additional parameters and a slight increase in training time. Furthermore, we have seen in Section 4.2 that in some cases the underlying data distribution can be adequately approximated by constant α and $\tilde{\alpha}$. Although not observed in this work, it is also plausible that the inclusion of these functions for more complex datasets may increase the risk of getting stuck in poor local minima during training, as incorrect shapes of these functions may promote poor representations (the shape of α and $\tilde{\alpha}$ affects the gradient of f and vice versa).

Finally, we want to emphasize that the mechanism that governs the observation pairs is highly dependent on the application and that the relationship between the latents may not be adequately described by a distance-based conditional as assumed in this work (Eq. (1)). However, we leave the exploration of methods suitable for other mechanisms to future work.

5 Conclusion

In this work, we propose a new theoretical framework of contrastive methods for learning disentangled representations. In contrast to previous research, our framework accounts for nonuniform marginal distributions of the factors of variation, allows for nonconvex latent spaces, and does not assume that these factors are statistically independent or conditionally independent given an auxiliary variable.

Our theory unveils that contrastive methods implicitly encode assumptions about the data generating process. We show empirically that even when these assumptions are partially violated, these methods learn to recover the true latent factors. This study provides further evidence that contrastive methods learn to approximately invert the underlying generative process, which may explain their remarkable success in many applications.

6 Acknowledgements

This work has been carried out as part of the AuSeSol-AI Project which is funded by Federal Ministry for the Environment, Nature Conservation, Nuclear Safety and Consumer Protection (BMUV) under the Grant 67KI21007F.

References

- [1] K. Ahuja, J. Hartford, and Y. Bengio. Weakly supervised representation learning with sparse perturbations. *arXiv preprint arXiv:2206.01101*, 2022.
- [2] P. Bachman, R. D. Hjelm, and W. Buchwalter. Learning representations by maximizing mutual information across views. *Advances in neural information processing systems*, 32, 2019.
- [3] H. B. Barlow, T. P. Kaushal, and G. J. Mitchison. Finding minimum entropy codes. *Neural Computation*, 1(3):412–423, 1989.
- [4] A. Ben-Israel. The change-of-variables formula using matrix volume. *SIAM Journal on Matrix Analysis and Applications*, 21(1):300–312, 1999.
- [5] J. Brehmer, P. De Haan, P. Lippe, and T. S. Cohen. Weakly supervised causal representation learning. *Advances in Neural Information Processing Systems*, 35:38319–38331, 2022.
- [6] L. E. Brouwer. Beweis der invarianz des n-dimensionalen gebiets. *Mathematische Annalen*, 71:305–313, 1911.
- [7] J.-F. Cardoso. Blind signal separation: statistical principles. *Proceedings of the IEEE*, 86(10):2009–2025, 1998.
- [8] T. Chen, S. Kornblith, M. Norouzi, and G. Hinton. A simple framework for contrastive learning of visual representations. In *International conference on machine learning*, pages 1597–1607. PMLR, 2020.
- [9] T. Chen, C. Luo, and L. Li. Intriguing properties of contrastive losses. *Advances in Neural Information Processing Systems*, 34:11834–11845, 2021.
- [10] E. Creager, D. Madras, J.-H. Jacobsen, M. Weis, K. Swersky, T. Pitassi, and R. Zemel. Flexibly fair representation learning by disentanglement. In *International conference on machine learning*, pages 1436–1445. PMLR, 2019.
- [11] C. Eastwood and C. K. Williams. A framework for the quantitative evaluation of disentangled representations. In *International Conference on Learning Representations*, 2018.
- [12] M. Fumero, L. Cosmo, S. Melzi, and E. Rodolà. Learning disentangled representations via product manifold projection. In *International conference on machine learning*, pages 3530–3540. PMLR, 2021.

- [13] L. Gao, Q. Mao, M. Dong, Y. Jing, and R. Chinnam. On learning disentangled representation for acoustic event detection. In *Proceedings of the 27th ACM International Conference on Multimedia*, pages 2006–2014, 2019.
- [14] A. Geiger, P. Lenz, and R. Urtasun. Are we ready for autonomous driving? the kitti vision benchmark suite. In *2012 IEEE conference on computer vision and pattern recognition*, pages 3354–3361. IEEE, 2012.
- [15] R. Geirhos, J.-H. Jacobsen, C. Michaelis, R. Zemel, W. Brendel, M. Bethge, and F. A. Wichmann. Shortcut learning in deep neural networks. *Nature Machine Intelligence*, 2(11):665–673, 2020.
- [16] L. Gresele, P. K. Rubenstein, A. Mehrjou, F. Locatello, and B. Schölkopf. The incomplete rosetta stone problem: Identifiability results for multi-view nonlinear ica. In *Uncertainty in Artificial Intelligence*, pages 217–227. PMLR, 2020.
- [17] L. Gresele, J. Von Kügelgen, V. Stimper, B. Schölkopf, and M. Besserve. Independent mechanism analysis, a new concept? *Advances in neural information processing systems*, 34:28233–28248, 2021.
- [18] M. Gutmann and A. Hyvärinen. Noise-contrastive estimation: A new estimation principle for unnormalized statistical models. In *Proceedings of the thirteenth international conference on artificial intelligence and statistics*, pages 297–304. JMLR Workshop and Conference Proceedings, 2010.
- [19] M. U. Gutmann and A. Hyvärinen. Noise-contrastive estimation of unnormalized statistical models, with applications to natural image statistics. *Journal of machine learning research*, 13(2), 2012.
- [20] J. Z. HaoChen, C. Wei, A. Gaidon, and T. Ma. Provable guarantees for self-supervised deep learning with spectral contrastive loss. *Advances in Neural Information Processing Systems*, 34:5000–5011, 2021.
- [21] K. He, H. Fan, Y. Wu, S. Xie, and R. Girshick. Momentum contrast for unsupervised visual representation learning. In *Proceedings of the IEEE/CVF conference on computer vision and pattern recognition*, pages 9729–9738, 2020.
- [22] D. Hendrycks and K. Gimpel. Gaussian error linear units (gelus). *arXiv preprint arXiv:1606.08415*, 2016.
- [23] R. D. Hjelm, A. Fedorov, S. Lavoie-Marchildon, K. Grewal, P. Bachman, A. Trischler, and Y. Bengio. Learning deep representations by mutual information estimation and maximization. *arXiv preprint arXiv:1808.06670*, 2018.
- [24] D. Horan, E. Richardson, and Y. Weiss. When is unsupervised disentanglement possible? *Advances in Neural Information Processing Systems*, 34:5150–5161, 2021.
- [25] A. Hyvärinen and H. Morioka. Unsupervised feature extraction by time-contrastive learning and nonlinear ica. *Advances in neural information processing systems*, 29, 2016.
- [26] A. Hyvärinen and H. Morioka. Nonlinear ica of temporally dependent stationary sources. In *Artificial Intelligence and Statistics*, pages 460–469. PMLR, 2017.
- [27] A. Hyvärinen and P. Pajunen. Nonlinear independent component analysis: Existence and uniqueness results. *Neural networks*, 12(3):429–439, 1999.
- [28] A. Hyvärinen, H. Sasaki, and R. E. Turner. Nonlinear ica using auxiliary variables and generalized contrastive learning. In *The 22nd International Conference on Artificial Intelligence and Statistics*, pages 859–868. PMLR, 2019.
- [29] R. Jozefowicz, O. Vinyals, M. Schuster, N. Shazeer, and Y. Wu. Exploring the limits of language modeling. *arXiv preprint arXiv:1602.02410*, 2016.
- [30] I. Khemakhem, D. Kingma, R. Monti, and A. Hyvarinen. Variational autoencoders and nonlinear ica: A unifying framework. In *International Conference on Artificial Intelligence and Statistics*, pages 2207–2217. PMLR, 2020.
- [31] I. Khemakhem, R. Monti, D. Kingma, and A. Hyvarinen. Ice-beem: Identifiable conditional energy-based deep models based on nonlinear ica. *Advances in Neural Information Processing Systems*, 33:12768–12778, 2020.
- [32] D. P. Kingma and J. Ba. Adam: A method for stochastic optimization. *arXiv preprint arXiv:1412.6980*, 2014.
- [33] D. P. Kingma and M. Welling. Auto-Encoding Variational Bayes. In *2nd International Conference on Learning Representations, ICLR 2014, Banff, AB, Canada, April 14-16, 2014, Conference Track Proceedings*, 2014.

- [34] D. Klindt, L. Schott, Y. Sharma, I. Ustuyuzhaninov, W. Brendel, M. Bethge, and D. Paiton. Towards nonlinear disentanglement in natural data with temporal sparse coding. *arXiv preprint arXiv:2007.10930*, 2020.
- [35] S. Lachapelle, P. Rodriguez, Y. Sharma, K. E. Everett, R. Le Priol, A. Lacoste, and S. Lacoste-Julien. Disentanglement via mechanism sparsity regularization: A new principle for nonlinear ica. In *Conference on Causal Learning and Reasoning*, pages 428–484. PMLR, 2022.
- [36] P. H. Le-Khac, G. Healy, and A. F. Smeaton. Contrastive representation learning: A framework and review. *Ieee Access*, 8:193907–193934, 2020.
- [37] C.-K. Li and W. So. Isometries of ℓ_p -norm. *The American mathematical monthly*, 101(5):452–453, 1994.
- [38] P. Lippe, S. Magliacane, S. Löwe, Y. M. Asano, T. Cohen, and S. Gavves. Citris: Causal identifiability from temporal intervened sequences. In *International Conference on Machine Learning*, pages 13557–13603. PMLR, 2022.
- [39] F. Locatello, G. Abbati, T. Rainforth, S. Bauer, B. Schölkopf, and O. Bachem. On the fairness of disentangled representations. *Advances in neural information processing systems*, 32, 2019.
- [40] F. Locatello, S. Bauer, M. Lucic, G. Raetsch, S. Gelly, B. Schölkopf, and O. Bachem. Challenging common assumptions in the unsupervised learning of disentangled representations. In *international conference on machine learning*, pages 4114–4124. PMLR, 2019.
- [41] F. Locatello, M. Tschannen, S. Bauer, G. Rätsch, B. Schölkopf, and O. Bachem. Disentangling factors of variation using few labels. *arXiv preprint arXiv:1905.01258*, 2019.
- [42] F. Locatello, B. Poole, G. Rätsch, B. Schölkopf, O. Bachem, and M. Tschannen. Weakly-supervised disentanglement without compromises. In *International Conference on Machine Learning*, pages 6348–6359. PMLR, 2020.
- [43] Z. Ma and M. Collins. Noise contrastive estimation and negative sampling for conditional models: Consistency and statistical efficiency. *arXiv preprint arXiv:1809.01812*, 2018.
- [44] P. Mankiewicz. On extension of isometries in normed linear spaces. *Bull. Acad. Pol. Sci., Sér. Sci. Math. Astron. Phys.*, 20:367–371, 1972.
- [45] A. Mnih and K. Kavukcuoglu. Learning word embeddings efficiently with noise-contrastive estimation. *Advances in neural information processing systems*, 26, 2013.
- [46] X. Nguyen, M. J. Wainwright, and M. I. Jordan. Estimating divergence functionals and the likelihood ratio by convex risk minimization. *IEEE Transactions on Information Theory*, 56(11):5847–5861, 2010.
- [47] A. v. d. Oord, Y. Li, and O. Vinyals. Representation learning with contrastive predictive coding. *arXiv preprint arXiv:1807.03748*, 2018.
- [48] K. Ridgeway and M. C. Mozer. Learning deep disentangled embeddings with the f-statistic loss. *Advances in neural information processing systems*, 31, 2018.
- [49] R. Shu, Y. Chen, A. Kumar, S. Ermon, and B. Poole. Weakly supervised disentanglement with guarantees. *arXiv preprint arXiv:1910.09772*, 2019.
- [50] A. Taleb and C. Jutten. Source separation in post-nonlinear mixtures. *IEEE Transactions on signal Processing*, 47(10):2807–2820, 1999.
- [51] Y. Tian, D. Krishnan, and P. Isola. Contrastive multiview coding. In *Computer Vision—ECCV 2020: 16th European Conference, Glasgow, UK, August 23–28, 2020, Proceedings, Part XI 16*, pages 776–794. Springer, 2020.
- [52] Y. Tian, C. Sun, B. Poole, D. Krishnan, C. Schmid, and P. Isola. What makes for good views for contrastive learning? *Advances in neural information processing systems*, 33:6827–6839, 2020.
- [53] M. Tschannen, J. Djolonga, P. K. Rubenstein, S. Gelly, and M. Lucic. On mutual information maximization for representation learning. *arXiv preprint arXiv:1907.13625*, 2019.
- [54] S. Van Steenkiste, F. Locatello, J. Schmidhuber, and O. Bachem. Are disentangled representations helpful for abstract visual reasoning? *Advances in Neural Information Processing Systems*, 32, 2019.

- [55] J. Von Kügelgen, Y. Sharma, L. Gresele, W. Brendel, B. Schölkopf, M. Besserve, and F. Locatello. Self-supervised learning with data augmentations provably isolates content from style. *Advances in neural information processing systems*, 34:16451–16467, 2021.
- [56] T. Wang and P. Isola. Understanding contrastive representation learning through alignment and uniformity on the hypersphere. In *International Conference on Machine Learning*, pages 9929–9939. PMLR, 2020.
- [57] R. Wobst. Isometrien in metrischen vektorräumen. *Studia Mathematica*, 1(54):41–54, 1975.
- [58] R. S. Zimmermann, Y. Sharma, S. Schneider, M. Bethge, and W. Brendel. Contrastive learning inverts the data generating process. In *International Conference on Machine Learning*, pages 12979–12990. PMLR, 2021.

A Proofs of the Theorems

In this section, we provide proofs of our theoretical claims. In many applications, the marginal distributions of the positive pairs $p_{\mathbf{x}}$ and $p_{\tilde{\mathbf{x}}}$ coincide, e.g., when \mathbf{x} and $\tilde{\mathbf{x}}$ are sampled as successive frames from a temporally stationary process. We consider here the case where $p_{\mathbf{x}}$ may also be different from $p_{\tilde{\mathbf{x}}}$ and the distribution of negative samples $p_{\mathbf{x}^-}$ is chosen to be nonzero on the support \mathcal{X} . In practice, given two batches of corresponding observations, it is often convenient to select the negative samples from the first, second, or both batches, resulting in $p_{\mathbf{x}^-} = p_{\mathbf{x}}$, $p_{\mathbf{x}^-} = p_{\tilde{\mathbf{x}}}$, or $p_{\mathbf{x}^-} = \frac{1}{2}(p_{\mathbf{x}} + p_{\tilde{\mathbf{x}}})$.

Lemma 1. *Let the data generating process follow Eq. 1 and g be differentiable and invertible. Further, assume that f and δ have universal approximation capability. Then for the optimal estimators of $\mathcal{L}_{\delta\text{-NCE}}(f, \delta)$, $\mathcal{L}_{\delta\text{-INCE}}(f, \delta; K)$, $\mathcal{L}_{\delta\text{-SCL}}(f, \delta)$ and $\mathcal{L}_{\delta\text{-NWJ}}(f, \delta)$, it holds that*

$$\delta(h(\mathbf{s}), h(\tilde{\mathbf{s}})) = -\log p_{\tilde{\mathbf{s}}|\mathbf{s}}(\tilde{\mathbf{s}}|\mathbf{s}) + p_{\mathbf{s}^-}(\tilde{\mathbf{s}}) + \gamma(\mathbf{s}), \quad (\text{S1})$$

where $h = f \circ g$ and γ is some function that only depends on \mathbf{s} .

Proof. We will show below for each loss function separately that the optimal estimators satisfy the form

$$\delta(f(\mathbf{x}), f(\tilde{\mathbf{x}})) = -\log p_{\tilde{\mathbf{x}}|\mathbf{x}}(\tilde{\mathbf{x}}|\mathbf{x}) + \log p_{\mathbf{x}^-}(\tilde{\mathbf{x}}) + \gamma_{\mathbf{x}}(\mathbf{x}), \quad (\text{S2})$$

where $\gamma_{\mathbf{x}}$ is a function that depends only on \mathbf{x} and is zero for all but $\mathcal{L}_{\delta\text{-INCE}}(f, \delta; K)$.

We can then use the fact that the data generating function g is injective and differentiable. This allows us to apply the probability transformations $p_{\tilde{\mathbf{x}}|\mathbf{x}}(\tilde{\mathbf{x}}|\mathbf{x}) = p_{\tilde{\mathbf{s}}|\mathbf{s}}(g^{-1}(\tilde{\mathbf{x}})|g^{-1}(\mathbf{x})) \text{vol } J_{g^{-1}}(\tilde{\mathbf{x}})$ and $p_{\mathbf{x}^-}(\tilde{\mathbf{x}}) = p_{\mathbf{s}^-}(g^{-1}(\tilde{\mathbf{x}})) \text{vol } J_{g^{-1}}(\tilde{\mathbf{x}})$, where $\text{vol } J_{g^{-1}}(\tilde{\mathbf{x}})$ is the product of the singular values of the Jacobian [4]. Thus, we obtain

$$\delta(f(\mathbf{x}), f(\tilde{\mathbf{x}})) = -\log p_{\tilde{\mathbf{s}}|\mathbf{s}}(g^{-1}(\tilde{\mathbf{x}})|g^{-1}(\mathbf{x})) + \log p_{\mathbf{s}^-}(g^{-1}(\tilde{\mathbf{x}})) + \gamma_{\mathbf{x}}(\mathbf{x}),$$

where the Jacobians nicely cancel. Finally, we substitute $\mathbf{x} = g(\mathbf{s})$ and $\tilde{\mathbf{x}} = g(\tilde{\mathbf{s}})$ and get

$$\delta(h(\mathbf{s}), h(\tilde{\mathbf{s}})) = -\log p_{\tilde{\mathbf{s}}|\mathbf{s}}(\tilde{\mathbf{s}}|\mathbf{s}) + \log p_{\mathbf{s}^-}(\tilde{\mathbf{s}}) + \gamma(\mathbf{s}),$$

where $\gamma(\mathbf{s}) = \gamma_{\mathbf{x}}(g(\mathbf{s}))$.

Part 1 (δ -NCE loss):

It is known that the NCE loss converges towards the log difference of the two data distributions of the positive and negative class [19, 26], that is

$$\delta(f(\mathbf{x}), f(\tilde{\mathbf{x}})) = -\log \frac{p_{\text{pos}}(\mathbf{x}, \tilde{\mathbf{x}})}{p_{\mathbf{x}}(\mathbf{x})p_{\mathbf{x}^-}(\tilde{\mathbf{x}})} = -\log p_{\tilde{\mathbf{x}}|\mathbf{x}}(\tilde{\mathbf{x}}|\mathbf{x}) + \log p_{\mathbf{x}^-}(\tilde{\mathbf{x}}).$$

Part 2 (δ -INCE loss):

The stated result can be obtained using Theorem 3.2 from Ma and Collins [43]. In addition, we give an alternative proof in Section B. Theorem 3.2 in [43] assumes (Assumption 2.1 in their work) that there exist functions f and δ such that for all $(\mathbf{x}, \tilde{\mathbf{x}}) \in \mathcal{X} \times \mathcal{X}$

$$\frac{p_{\tilde{\mathbf{x}}|\mathbf{x}}(\tilde{\mathbf{x}}|\mathbf{x})}{p_{\mathbf{x}^-}(\tilde{\mathbf{x}})} = \frac{1}{Z(\mathbf{x})} e^{-\delta(f(\mathbf{x}), f(\tilde{\mathbf{x}}))}, \quad (\text{S3})$$

where $Z(\mathbf{x}) = \mathbb{E}_{\tilde{\mathbf{x}}} e^{-\delta(f(\mathbf{x}), f(\tilde{\mathbf{x}}))}$. This assumption is satisfied since we optimize both f and δ using universal function approximators. Then the theorem states that in the limit of infinite data, this relation holds for the global optimum when we optimize the InfoNCE loss. To obtain their notation, simply replace $\mathbf{y} = \tilde{\mathbf{x}}$ and $s(\mathbf{x}, \mathbf{y}) = \log p_{\mathbf{x}^-}(\tilde{\mathbf{x}}) - \delta(f(\mathbf{x}), f(\tilde{\mathbf{x}}))$. Therefore, we get $\delta(f(\mathbf{x}), f(\tilde{\mathbf{x}})) = -\log p_{\tilde{\mathbf{x}}|\mathbf{x}}(\tilde{\mathbf{x}}|\mathbf{x}) + \log p_{\mathbf{x}^-}(\tilde{\mathbf{x}}) + \gamma_{\mathbf{x}}(\mathbf{x})$ with $\gamma_{\mathbf{x}}(\mathbf{x}) = -\log Z(\mathbf{x})$.

Part 3 (δ -SCL loss):

To simplify the notation, we substitute $\psi(\mathbf{x}, \tilde{\mathbf{x}}) = -\delta(f(\mathbf{x}), f(\tilde{\mathbf{x}}))$ in the δ -SCL loss and obtain

$$\tilde{\mathcal{L}}_{\delta\text{-SCL}}(\psi) = \mathbb{E}_{\substack{(\mathbf{x}, \tilde{\mathbf{x}}) \\ \sim p_{\text{pos}}}} -2e^{\psi(\mathbf{x}, \tilde{\mathbf{x}})} + \mathbb{E}_{\substack{\mathbf{x} \sim p_{\mathbf{x}} \\ \mathbf{x}^- \sim p_{\mathbf{x}^-}}} e^{2\psi(\mathbf{x}, \mathbf{x}^-)}. \quad (\text{S4})$$

First we derive the Taylor series of $\tilde{\mathcal{L}}_{\delta\text{-SCL}}$:

$$\begin{aligned} \tilde{\mathcal{L}}_{\delta\text{-SCL}}(\psi + \epsilon\eta) &= \tilde{\mathcal{L}}_{\delta\text{-SCL}}(\psi) + 2\epsilon \left[\mathbb{E}_{\substack{(\mathbf{x}, \tilde{\mathbf{x}}) \\ \sim p_{\text{pos}}}} - e^{\psi(\mathbf{x}, \tilde{\mathbf{x}})} \eta(\mathbf{x}, \tilde{\mathbf{x}}) + \mathbb{E}_{\substack{\mathbf{x} \sim p_{\mathbf{x}} \\ \mathbf{x}^- \sim p_{\mathbf{x}^-}}} e^{2\psi(\mathbf{x}, \mathbf{x}^-)} \eta(\mathbf{x}, \mathbf{x}^-) \right] \\ &\quad + \epsilon^2 \left[\mathbb{E}_{\substack{(\mathbf{x}, \tilde{\mathbf{x}}) \\ \sim p_{\text{pos}}}} - e^{\psi(\mathbf{x}, \tilde{\mathbf{x}})} \eta(\mathbf{x}, \tilde{\mathbf{x}})^2 + 2 \mathbb{E}_{\substack{\mathbf{x} \sim p_{\mathbf{x}} \\ \mathbf{x}^- \sim p_{\mathbf{x}^-}}} e^{2\psi(\mathbf{x}, \mathbf{x}^-)} \eta(\mathbf{x}, \mathbf{x}^-)^2 \right] + \mathcal{O}(\epsilon^3). \end{aligned} \quad (\text{S5})$$

A necessary optimality condition is that in the expansion of $\tilde{\mathcal{L}}_{\delta\text{-SCL}}$, the term of order ϵ is zero for any perturbation η . We have

$$\begin{aligned} 0 &= \mathbb{E}_{\substack{(\mathbf{x}, \tilde{\mathbf{x}}) \\ \sim p_{\text{pos}}}} - e^{\psi(\mathbf{x}, \tilde{\mathbf{x}})} \eta(\mathbf{x}, \tilde{\mathbf{x}}) + \mathbb{E}_{\substack{\mathbf{x} \sim p_{\mathbf{x}} \\ \mathbf{x}^- \sim p_{\mathbf{x}^-}}} e^{2\psi(\mathbf{x}, \mathbf{x}^-)} \eta(\mathbf{x}, \mathbf{x}^-) \\ &= \int p_{\mathbf{x}}(\mathbf{x}) p_{\mathbf{x}^-}(\mathbf{x}^-) e^{2\psi(\mathbf{x}, \mathbf{x}^-)} \eta(\mathbf{x}, \mathbf{x}^-) d\mathbf{x} d\mathbf{x}^- - \int p_{\text{pos}}(\mathbf{x}, \tilde{\mathbf{x}}) e^{\psi(\mathbf{x}, \tilde{\mathbf{x}})} \eta(\mathbf{x}, \tilde{\mathbf{x}}) d\mathbf{x} d\tilde{\mathbf{x}} \\ &= \int p_{\mathbf{x}}(\mathbf{x}) p_{\mathbf{x}^-}(\tilde{\mathbf{x}}) e^{2\psi(\mathbf{x}, \tilde{\mathbf{x}})} \eta(\mathbf{x}, \tilde{\mathbf{x}}) d\mathbf{x} d\tilde{\mathbf{x}} - \int p_{\text{pos}}(\mathbf{x}, \tilde{\mathbf{x}}) e^{\psi(\mathbf{x}, \tilde{\mathbf{x}})} \eta(\mathbf{x}, \tilde{\mathbf{x}}) d\mathbf{x} d\tilde{\mathbf{x}} \\ &= \int \left(p_{\mathbf{x}}(\mathbf{x}) p_{\mathbf{x}^-}(\tilde{\mathbf{x}}) e^{2\psi(\mathbf{x}, \tilde{\mathbf{x}})} - p_{\text{pos}}(\mathbf{x}, \tilde{\mathbf{x}}) e^{\psi(\mathbf{x}, \tilde{\mathbf{x}})} \right) \eta(\mathbf{x}, \tilde{\mathbf{x}}) d\mathbf{x} d\tilde{\mathbf{x}}. \end{aligned}$$

This term vanishes if and only if

$$e^{\psi(\mathbf{x}, \tilde{\mathbf{x}})} = \frac{p_{\text{pos}}(\mathbf{x}, \tilde{\mathbf{x}})}{p_{\mathbf{x}}(\mathbf{x}) p_{\mathbf{x}^-}(\tilde{\mathbf{x}})},$$

that is $\psi^*(\mathbf{x}, \tilde{\mathbf{x}}) = \log p_{\tilde{\mathbf{x}}|\mathbf{x}}(\tilde{\mathbf{x}}|\mathbf{x}) - \log p_{\mathbf{x}^-}(\tilde{\mathbf{x}})$.

To verify that the critical point is indeed a minimizer, we insert the solution back into Eq. S5 and check if the order ϵ^2 term is strictly positive for any direction η . This leads to

$$\begin{aligned} \tilde{\mathcal{L}}_{\delta\text{-SCL}}(\psi^* + \epsilon\eta) &= \tilde{\mathcal{L}}_{\delta\text{-SCL}}(\psi^*) \\ &\quad + \epsilon^2 \left[\mathbb{E}_{\substack{(\mathbf{x}, \tilde{\mathbf{x}}) \\ \sim p_{\text{pos}}}} - \frac{p_{\text{pos}}(\mathbf{x}, \tilde{\mathbf{x}})}{p_{\mathbf{x}}(\mathbf{x}) p_{\mathbf{x}^-}(\tilde{\mathbf{x}})} \eta(\mathbf{x}, \tilde{\mathbf{x}})^2 + 2 \mathbb{E}_{\substack{\mathbf{x} \sim p_{\mathbf{x}} \\ \mathbf{x}^- \sim p_{\mathbf{x}^-}}} \left(\frac{p_{\text{pos}}(\mathbf{x}, \mathbf{x}^-)}{p_{\mathbf{x}}(\mathbf{x}) p_{\mathbf{x}^-}(\mathbf{x}^-)} \right)^2 \eta(\mathbf{x}, \mathbf{x}^-)^2 \right] + \mathcal{O}(\epsilon^3). \end{aligned} \quad (\text{S6})$$

The order ϵ^2 term can be simplified to

$$\int \frac{p_{\text{pos}}(\mathbf{x}, \tilde{\mathbf{x}})^2}{p_{\mathbf{x}}(\mathbf{x}) p_{\mathbf{x}^-}(\tilde{\mathbf{x}})} \eta(\mathbf{x}, \tilde{\mathbf{x}})^2 d\mathbf{x} d\tilde{\mathbf{x}},$$

which is clearly positive for any direction η . Thus, $\tilde{\mathcal{L}}_{\delta\text{-SCL}}$ reaches indeed a minimum at ψ^* , or in terms of δ and f , we have $\delta(f(\mathbf{x}), f(\tilde{\mathbf{x}})) = -\log p_{\tilde{\mathbf{x}}|\mathbf{x}}(\tilde{\mathbf{x}}|\mathbf{x}) + \log p_{\mathbf{x}^-}(\tilde{\mathbf{x}})$.

Part 4 (δ -NWJ loss):

The proof for $\mathcal{L}_{\delta\text{-NWJ}}$ is analogous to $\mathcal{L}_{\delta\text{-SCL}}$. We use the same substitution as in the last part, i.e., $\psi(\mathbf{x}, \tilde{\mathbf{x}}) = -\delta(f(\mathbf{x}), f(\tilde{\mathbf{x}}))$, and get

$$\tilde{\mathcal{L}}_{\delta\text{-NWJ}}(\psi) = \mathbb{E}_{\substack{(\mathbf{x}, \tilde{\mathbf{x}}) \\ \sim p_{\text{pos}}}} -\psi(\mathbf{x}, \tilde{\mathbf{x}}) + \mathbb{E}_{\substack{\mathbf{x} \sim p_{\mathbf{x}} \\ \mathbf{x}^- \sim p_{\mathbf{x}^-}}} e^{\psi(\mathbf{x}, \mathbf{x}^-)}. \quad (\text{S7})$$

The Taylor expansion of $\tilde{\mathcal{L}}_{\delta\text{-NWJ}}$ is given by

$$\begin{aligned} \tilde{\mathcal{L}}_{\delta\text{-NWJ}}(\psi + \epsilon\eta) &= \tilde{\mathcal{L}}_{\delta\text{-NWJ}}(\psi) + \epsilon \left[\mathbb{E}_{\substack{(\mathbf{x}, \tilde{\mathbf{x}}) \\ \sim p_{\text{pos}}}} -\eta(\mathbf{x}, \tilde{\mathbf{x}}) + \mathbb{E}_{\substack{\mathbf{x} \sim p_{\mathbf{x}} \\ \mathbf{x}^- \sim p_{\mathbf{x}^-}}} e^{\psi(\mathbf{x}, \mathbf{x}^-)} \eta(\mathbf{x}, \mathbf{x}^-) \right] \\ &\quad + \frac{1}{2} \epsilon^2 \mathbb{E}_{\substack{\mathbf{x} \sim p_{\mathbf{x}} \\ \mathbf{x}^- \sim p_{\mathbf{x}^-}}} e^{\psi(\mathbf{x}, \mathbf{x}^-)} \eta(\mathbf{x}, \mathbf{x}^-)^2 + \mathcal{O}(\epsilon^3). \end{aligned} \quad (\text{S8})$$

Again, the term of order ϵ is zero at $\psi^*(\mathbf{x}, \tilde{\mathbf{x}}) = \log p_{\tilde{\mathbf{x}}|\mathbf{x}}(\tilde{\mathbf{x}}|\mathbf{x}) - \log p_{\mathbf{x}^-}(\tilde{\mathbf{x}})$ and we directly see that the ϵ^2 term is strictly positive for any direction η . \square

Lemma 2. *Let the data generating process follow Eq. 1, where d is a semi-metric (i.e., the triangle inequality does not necessarily hold), and \mathcal{S} is open. Let us further assume that δ has the form as in Eq. 2 and satisfies $\delta(h(\mathbf{s}), h(\tilde{\mathbf{s}})) = -\log p_{\tilde{\mathbf{s}}|\mathbf{s}}(\tilde{\mathbf{s}}|\mathbf{s}) + \log p_{\mathbf{s}^-}(\tilde{\mathbf{s}}) + \gamma(\mathbf{s})$. Then, for the optimal estimators of the contrastive losses presented above, h is a homeomorphism between \mathcal{S} and $h(\mathcal{S})$.*

Proof. After inserting $p_{\tilde{\mathbf{s}}|\mathbf{s}}(\tilde{\mathbf{s}}|\mathbf{s})$ from Eq. 1 and δ from Eq. 2, we obtain

$$d(h(\mathbf{s}), h(\tilde{\mathbf{s}})) + \alpha(h(\mathbf{s})) + \tilde{\alpha}(h(\tilde{\mathbf{s}})) = d(\mathbf{s}, \tilde{\mathbf{s}}) - \log Q(\tilde{\mathbf{s}}) + \log Z(\mathbf{s}) + \log p_{\mathbf{s}^-}(\tilde{\mathbf{s}}) + \gamma(\mathbf{s}). \quad (\text{S9})$$

This must also hold for all $\mathbf{s}, \tilde{\mathbf{s}}$, including $\mathbf{s} = \tilde{\mathbf{s}}$, and since $d(\mathbf{s}, \mathbf{s}) = d(h(\mathbf{s}), h(\mathbf{s}))$, we have

$$\alpha(h(\mathbf{s})) + \tilde{\alpha}(h(\mathbf{s})) = -\log Q(\mathbf{s}) + \log Z(\mathbf{s}) + \log p_{\mathbf{s}^-}(\mathbf{s}) + \gamma(\mathbf{s}). \quad (\text{S10})$$

Now we subtract the last two equations and get

$$d(h(\mathbf{s}), h(\tilde{\mathbf{s}})) + \tilde{\alpha}(h(\tilde{\mathbf{s}})) - \tilde{\alpha}(h(\mathbf{s})) = d(\mathbf{s}, \tilde{\mathbf{s}}) - \log Q(\tilde{\mathbf{s}}) + \log Q(\mathbf{s}) + \log p_{\mathbf{s}^-}(\tilde{\mathbf{s}}) - \log p_{\mathbf{s}^-}(\mathbf{s}). \quad (\text{S11})$$

Because of the symmetry of d we can conclude

$$d(h(\mathbf{s}), h(\tilde{\mathbf{s}})) = d(\mathbf{s}, \tilde{\mathbf{s}}). \quad (\text{S12})$$

If h were not injective, there would be some $\mathbf{s} \neq \tilde{\mathbf{s}}$ with $h(\mathbf{s}) = h(\tilde{\mathbf{s}})$. This would imply that $0 = d(h(\mathbf{s}), h(\tilde{\mathbf{s}})) = d(\mathbf{s}, \tilde{\mathbf{s}}) > 0$, which is a contradiction.

Since h is an injective continuous mapping and \mathcal{S} is open, h is a homeomorphism due to the domain invariance theorem (see [6]). \square

From Eq. (S9), we also see that $\tilde{\alpha} \circ h = \log p_{\mathbf{s}^-} - \log Q$ and, except for $\mathcal{L}_{\delta\text{-INCE}}(f, \delta; K)$, $\alpha \circ h = \log Z$.

Before we continue, let us recall an important theorem by Mankiewicz [44] and the definition of 2-extremal points [57].

Theorem A. (Mankiewicz, 1972) *Suppose \mathcal{X} and \mathcal{Y} are real normed vector spaces, \mathcal{U} a nonempty subset of \mathcal{X} , and let $f : \mathcal{U} \rightarrow f(\mathcal{U})$ be a surjective isometry, where $f(\mathcal{U})$ is a subset of \mathcal{Y} . If either both \mathcal{U} and $f(\mathcal{U})$ are convex bodies or open and connected, then f can be uniquely extended to an affine isometry from \mathcal{X} to \mathcal{Y} .*

Proof. See [44]. \square

Definition 1. *As a 2-extremal point of a set \mathcal{U} of a vector space we denote each element $\mathbf{x} \in \mathcal{U}$ such that from $\mathbf{u}, \mathbf{u}' \in \mathcal{U}$ and $\mathbf{u} + \mathbf{u}' = 2\mathbf{x}$ follows $\mathbf{u} = \mathbf{u}' = \mathbf{x}$.*

Theorem 1 (Weak identifiability). *Let $\mathcal{S} \subseteq \mathbb{R}^n$ be open and connected, $\mathcal{X} \subseteq \mathbb{R}^m$, and $g : \mathcal{S} \rightarrow \mathcal{X}$ invertible and differentiable. Let us further assume that the observed data satisfy the generative model given in Eq. (1). If $d = \hat{d}$ has one of the following properties:*

- (i) *there exists a function $\xi : \mathbb{R}^+ \rightarrow \mathbb{R}^+$, such that $\xi \circ d$ is a norm-induced metric,*
- (ii) *$d(\mathbf{s}, \tilde{\mathbf{s}}) = \sum_i d_i(|s_i - \tilde{s}_i|)$, where each d_i is continuous and strictly increasing,*

then the optimal estimator of any of the contrastive losses presented above identifies the true latent factors up to affine transformations, i.e., $h = f \circ g$ is an affine mapping.

Proof. By Lemma 1 and Lemma 2, h is injective. Furthermore, since h is continuous and \mathcal{S} is open, $h(\mathcal{S})$ is also open. Additionally, $h(\mathcal{S})$ is connected because \mathcal{S} is connected.

Assume that condition (i) holds. Then, h is an isometry and we can apply Mankiewicz's theorem, which tells us that h is an affine mapping.

Let us now consider condition (ii). We show that h is affine using central ideas of Lemma 2 in [57]. Let \mathbf{s}_0 be a 2-extremal point of $\mathcal{B}_r = \{\mathbf{s} \in \mathbb{R}^n : d(0, \mathbf{s}) \leq r\}$. Then $-\mathbf{s}_0$ is also a 2-extremal point of \mathcal{B}_r , since d is symmetric. Now define $\phi(\mathbf{s}) = h(\mathbf{s}) - h(0)$ and $\mathcal{A} = (\mathcal{B}_r + \mathbf{s} + \mathbf{s}_0) \cap (\mathcal{B}_r + \mathbf{s} - \mathbf{s}_0)$ for $\mathbf{s} \in \mathcal{S}$. It is straightforward to verify that \mathbf{s} is the only element contained in \mathcal{A} . Since h is injective and d is translation invariant, we have

$$\phi(\mathcal{A}) = (\phi(\mathcal{B}_r) + \phi(\mathbf{s} + \mathbf{s}_0)) \cap (\phi(\mathcal{B}_r) + \phi(\mathbf{s} - \mathbf{s}_0)),$$

and because d is symmetric we can conclude

$$\phi(\mathbf{s}) = \frac{1}{2} (\phi(\mathbf{s} + \mathbf{s}_0) + \phi(\mathbf{s} - \mathbf{s}_0)). \quad (\text{S13})$$

It is obvious that for the standard basis vectors $\mathbf{e}_i \in \mathbb{R}^n$ each $a_i \mathbf{e}_i$ with $d(0, a_i \mathbf{e}_i) = r$ is a 2-extremal point of \mathcal{B}_r since each d_i is strictly monotonically increasing. For each pair of different $\mathbf{s}, \mathbf{s}' \in \mathcal{B}_r$ with $\mathbf{s} + \mathbf{s}' = 2a_i \mathbf{e}_i$ we would have either $s_i = s'_i = a_i$ and for at least one coordinate $j \neq i$ $-s_j = s'_j \neq 0$ or one of \mathbf{s}, \mathbf{s}' would have a higher value than a_i at the i -th coordinate. So in both cases \mathbf{s} or \mathbf{s}' would lie outside \mathcal{B}_r , which is a contradiction. It follows from Eq. (S13) that straight lines in the direction of one of the standard basis vectors are mapped to straight lines, i.e., $\phi(\mathbf{s} + a_i \mathbf{e}_i) = \phi(\mathbf{s}) + a_i (\phi(\mathbf{s} + \mathbf{e}_i) - \phi(\mathbf{s}))$.

Furthermore we have

$$d(0, a_i \mathbf{e}_i) = d(\mathbf{s}, \mathbf{s} + a_i \mathbf{e}_i) = d(\phi(\mathbf{s}), \phi(\mathbf{s} + a_i \mathbf{e}_i)) = d(0, a_i (\phi(\mathbf{s} + \mathbf{e}_i) - \phi(\mathbf{s}))),$$

and since the distance does not depend on \mathbf{s} , we obtain $\phi(\mathbf{s} + a_i \mathbf{e}_i) = \phi(\mathbf{s}) + a_i \phi(\mathbf{e}_i)$. After iterating over all \mathbf{e}_i , we can conclude $\phi(\mathbf{s} + \sum_i a_i \mathbf{e}_i) = \phi(\mathbf{s}) + \sum_i a_i \phi(\mathbf{e}_i)$. □

Theorem 2 (Strong identifiability). *Assume that all conditions in Theorem 1 are satisfied. Let the function d in Eq. (1) be defined by*

$$d(\mathbf{s}, \tilde{\mathbf{s}}) = \sum_i (|s_i - \tilde{s}_i| / \sigma_i)^\beta, \quad (\text{S14})$$

with $\beta \in (0, 2) \cup (2, \infty)$ and $\sigma_i > 0$ for all i , then $h = f \circ g$ is a generalized permutation matrix, i.e., a composition of a permutation and element-wise scaling and sign flips.

Proof. From Theorem 1 we know that $h(\mathbf{s}) = \mathbf{A}\mathbf{s} + \mathbf{b}$. For $p \geq 1$ we can define $\xi(x) = x^{1/p}$. Thus, h preserves the p -norm. In this case it has already been proved that \mathbf{A} is a generalized permutation matrix (see, for example, [37]).

Let us now look at the case $0 < p < 1$. We denote the element in the i -th row and j -th column of \mathbf{A} with a_{ij} . For any standard basis vector \mathbf{e}_i , it holds

$$1 = d(0, \mathbf{e}_i) = d(0, \mathbf{A}\mathbf{e}_i) = \sum_j |a_{ji}|^p.$$

Similarly for two different basis vectors \mathbf{e}_i and \mathbf{e}_j , we have

$$2 = d(0, \mathbf{e}_i + \mathbf{e}_j) = d(0, \mathbf{A}(\mathbf{e}_i + \mathbf{e}_j)) = \sum_k |a_{ki} + a_{kj}|^p \leq \sum_k |a_{ki}|^p + \sum_k |a_{kj}|^p.$$

The last part is due to the triangle inequality. This implies that a_{ki} and a_{kj} must have the same sign or at least one of them must be zero.

On the other hand we have

$$2 = d(0, \mathbf{e}_i - \mathbf{e}_j) = d(0, \mathbf{A}(\mathbf{e}_i - \mathbf{e}_j)) = \sum_k |a_{ki} - a_{kj}|^p \leq \sum_k |a_{ki}|^p + \sum_k |a_{kj}|^p.$$

Therefore, a_{ki} and a_{kj} must have different signs or at least one of them must be zero. Taken together, this means that each row of \mathbf{A} can have at most one nonzero entry. And since \mathbf{A} is invertible, it is a generalized permutation matrix. □

B Alternative Convergence Proof for the δ -INCE Loss

Proof. We first make the substitution $\psi(\mathbf{x}, \tilde{\mathbf{x}}) = -\delta(f(\mathbf{x}), f(\tilde{\mathbf{x}}))$ and replace $\tilde{\mathbf{x}}$ with $\tilde{\mathbf{x}}_0$ and \mathbf{x}_i^- with $\tilde{\mathbf{x}}_i$ for $i \neq 0$. The δ -INCE loss can then be formulated as

$$\tilde{\mathcal{L}}_{\delta\text{-INCE}}(\psi) = \mathbb{E}_{\substack{(\mathbf{x}, \tilde{\mathbf{x}}_0) \sim p_{\text{pos}} \\ \{\tilde{\mathbf{x}}_i\}_{i=1}^K \stackrel{\text{i.i.d.}}{\sim} p_{\mathbf{x}^-}}} - \log \frac{e^{\psi(\mathbf{x}, \tilde{\mathbf{x}}_0)}}{\sum_{i=0}^K e^{\psi(\mathbf{x}, \tilde{\mathbf{x}}_i)}}. \quad (\text{S15})$$

The logarithmic term can be also written as

$$r(\psi) = -\log \frac{e^{\psi(\mathbf{x}, \tilde{\mathbf{x}}_0)}}{\sum_i e^{\psi(\mathbf{x}, \tilde{\mathbf{x}}_i)}} = -\psi(\mathbf{x}, \tilde{\mathbf{x}}_0) + \log \sum_i e^{\psi(\mathbf{x}, \tilde{\mathbf{x}}_i)}$$

and has the following Gateaux derivatives:

$$\begin{aligned} \left. \frac{d}{d\epsilon} r(\psi + \epsilon\eta) \right|_{\epsilon=0} &= \frac{\sum_j e^{\psi(\mathbf{x}, \tilde{\mathbf{x}}_j)} (\eta(\mathbf{x}, \tilde{\mathbf{x}}_j) - \eta(\mathbf{x}, \tilde{\mathbf{x}}_0))}{\sum_i e^{\psi(\mathbf{x}, \tilde{\mathbf{x}}_i)}} \\ \left. \frac{d^2}{d\epsilon^2} r(\psi + \epsilon\eta) \right|_{\epsilon=0} &= \frac{\sum_i e^{\psi(\mathbf{x}, \tilde{\mathbf{x}}_i)} \sum_j e^{\psi(\mathbf{x}, \tilde{\mathbf{x}}_j)} \eta(\mathbf{x}, \tilde{\mathbf{x}}_j)^2 - \left(\sum_j e^{\psi(\mathbf{x}, \tilde{\mathbf{x}}_j)} \eta(\mathbf{x}, \tilde{\mathbf{x}}_j) \right)^2}{\left(\sum_i e^{\psi(\mathbf{x}, \tilde{\mathbf{x}}_i)} \right)^2}. \end{aligned}$$

Thus, the Taylor series of $\tilde{\mathcal{L}}_{\delta\text{-INCE}}$ is given by

$$\begin{aligned} \tilde{\mathcal{L}}_{\delta\text{-INCE}}(\psi + \epsilon\eta) &= \tilde{\mathcal{L}}_{\delta\text{-INCE}}(\psi) + \epsilon \mathbb{E}_{\substack{(\mathbf{x}, \tilde{\mathbf{x}}_0) \sim p_{\text{pos}} \\ \{\tilde{\mathbf{x}}_i\}_{i=1}^K \stackrel{\text{i.i.d.}}{\sim} p_{\mathbf{x}^-}}} \frac{\sum_j e^{\psi(\mathbf{x}, \tilde{\mathbf{x}}_j)} (\eta(\mathbf{x}, \tilde{\mathbf{x}}_j) - \eta(\mathbf{x}, \tilde{\mathbf{x}}_0))}{\sum_i e^{\psi(\mathbf{x}, \tilde{\mathbf{x}}_i)}} \\ &+ \frac{1}{2} \epsilon^2 \mathbb{E}_{\substack{(\mathbf{x}, \tilde{\mathbf{x}}_0) \sim p_{\text{pos}} \\ \{\tilde{\mathbf{x}}_i\}_{i=1}^K \stackrel{\text{i.i.d.}}{\sim} p_{\mathbf{x}^-}}} \frac{\sum_i e^{\psi(\mathbf{x}, \tilde{\mathbf{x}}_i)} \sum_j e^{\psi(\mathbf{x}, \tilde{\mathbf{x}}_j)} \eta(\mathbf{x}, \tilde{\mathbf{x}}_j)^2 - \left(\sum_j e^{\psi(\mathbf{x}, \tilde{\mathbf{x}}_j)} \eta(\mathbf{x}, \tilde{\mathbf{x}}_j) \right)^2}{\left(\sum_i e^{\psi(\mathbf{x}, \tilde{\mathbf{x}}_i)} \right)^2} + \mathcal{O}(\epsilon^3). \end{aligned} \quad (\text{S16})$$

A sufficient condition for $\tilde{\mathcal{L}}_{\delta\text{-INCE}}$ to reach an optimum is that the term of order ϵ vanishes and the term of order ϵ^2 is strictly positive for all directions η . Note that the choice of the variable $\tilde{\mathbf{x}}_0$ for the positive example was arbitrary. By iteratively renaming the positive example to $\tilde{\mathbf{x}}_k$ for $k = 0, \dots, K$ and calculating the mean, we can transform the term of order ϵ in the following way:

$$\begin{aligned} &\mathbb{E}_{\substack{(\mathbf{x}, \tilde{\mathbf{x}}_0) \sim p_{\text{pos}} \\ \{\tilde{\mathbf{x}}_i\}_{i=1}^K \stackrel{\text{i.i.d.}}{\sim} p_{\mathbf{x}^-}}} \frac{\sum_j e^{\psi(\mathbf{x}, \tilde{\mathbf{x}}_j)} (\eta(\mathbf{x}, \tilde{\mathbf{x}}_j) - \eta(\mathbf{x}, \tilde{\mathbf{x}}_0))}{\sum_i e^{\psi(\mathbf{x}, \tilde{\mathbf{x}}_i)}} \\ &= \frac{1}{K+1} \sum_{k=0}^K \mathbb{E}_{\substack{(\mathbf{x}, \tilde{\mathbf{x}}_k) \sim p_{\text{pos}} \\ \{\tilde{\mathbf{x}}_i\}_{i \neq k} \stackrel{\text{i.i.d.}}{\sim} p_{\mathbf{x}^-}}} \frac{\sum_j e^{\psi(\mathbf{x}, \tilde{\mathbf{x}}_j)} (\eta(\mathbf{x}, \tilde{\mathbf{x}}_j) - \eta(\mathbf{x}, \tilde{\mathbf{x}}_k))}{\sum_i e^{\psi(\mathbf{x}, \tilde{\mathbf{x}}_i)}}. \end{aligned} \quad (\text{S17})$$

This expression vanishes for all η if and only if

$$\prod_l p_{\mathbf{x}^-}(\tilde{\mathbf{x}}_l) \sum_k p(\mathbf{x} | \tilde{\mathbf{x}}_k) \frac{\sum_j e^{\psi(\mathbf{x}, \tilde{\mathbf{x}}_j)} (\eta(\mathbf{x}, \tilde{\mathbf{x}}_j) - \eta(\mathbf{x}, \tilde{\mathbf{x}}_k))}{\sum_i e^{\psi(\mathbf{x}, \tilde{\mathbf{x}}_i)}} = 0,$$

which can be simplified to

$$\sum_k p(\mathbf{x}|\tilde{\mathbf{x}}_k) \sum_j e^{\psi(\mathbf{x}, \tilde{\mathbf{x}}_j)} \eta(\mathbf{x}, \tilde{\mathbf{x}}_j) = \sum_j e^{\psi(\mathbf{x}, \tilde{\mathbf{x}}_j)} \sum_k p(\mathbf{x}|\tilde{\mathbf{x}}_k) \eta(\mathbf{x}, \tilde{\mathbf{x}}_k).$$

Since this must hold for all $\tilde{\mathbf{x}}_i$ and arbitrary η , we obtain

$$\frac{e^{\psi(\mathbf{x}, \tilde{\mathbf{x}}_i)}}{\sum_j e^{\psi(\mathbf{x}, \tilde{\mathbf{x}}_j)}} = \frac{p(\mathbf{x}|\tilde{\mathbf{x}}_i)}{\sum_j p(\mathbf{x}|\tilde{\mathbf{x}}_j)}.$$

Obviously, for any solution ψ^* , the function $\psi^*(\mathbf{x}, \tilde{\mathbf{x}}) + c(\mathbf{x})$ is also a solution, where $c(\mathbf{x})$ is a function that only depends on \mathbf{x} . Thus, we finally obtain $\psi^*(\mathbf{x}, \tilde{\mathbf{x}}) = \log p(\mathbf{x}|\tilde{\mathbf{x}}) + c(\mathbf{x})$ or equivalently $\psi^*(\mathbf{x}, \tilde{\mathbf{x}}) = \log p(\tilde{\mathbf{x}}|\mathbf{x}) - \log p_{\mathbf{x}^-}(\tilde{\mathbf{x}}) + \gamma_{\mathbf{x}}(\mathbf{x})$ using Bayes' theorem, where $\gamma_{\mathbf{x}}(\mathbf{x}) = c(\mathbf{x}) + \log p_{\mathbf{x}}(\mathbf{x})$.

Plugging this back into $\tilde{\mathcal{L}}_{\delta\text{-INCE}}$ we get

$$\begin{aligned} \tilde{\mathcal{L}}_{\delta\text{-INCE}}(\psi^* + \epsilon\eta) &= \tilde{\mathcal{L}}_{\delta\text{-INCE}}(\psi^*) \\ &+ \frac{1}{2}\epsilon^2 \mathbb{E}_{\substack{(\mathbf{x}, \tilde{\mathbf{x}}_0) \sim p_{\text{pos}} \\ \{\tilde{\mathbf{x}}_i\}_{i=1}^K \stackrel{\text{i.i.d.}}{\sim} p_{\mathbf{x}^-}}} \frac{\sum_i p(\mathbf{x}|\tilde{\mathbf{x}}_i) \sum_j p(\mathbf{x}|\tilde{\mathbf{x}}_j) \eta(\mathbf{x}, \tilde{\mathbf{x}}_j)^2 - \left(\sum_j p(\mathbf{x}|\tilde{\mathbf{x}}_j) \eta(\mathbf{x}, \tilde{\mathbf{x}}_j)\right)^2}{\left(\sum_i p(\mathbf{x}|\tilde{\mathbf{x}}_i)\right)^2} + \mathcal{O}(\epsilon^3). \end{aligned} \tag{S18}$$

The term of order ϵ^2 can be rearranged into

$$\frac{1}{4}\epsilon^2 \mathbb{E}_{\substack{(\mathbf{x}, \tilde{\mathbf{x}}_0) \sim p_{\text{pos}} \\ \{\tilde{\mathbf{x}}_i\}_{i=1}^K \stackrel{\text{i.i.d.}}{\sim} p_{\mathbf{x}^-}}} \frac{\sum_i \sum_j p(\mathbf{x}|\tilde{\mathbf{x}}_i) p(\mathbf{x}|\tilde{\mathbf{x}}_j) (\eta(\mathbf{x}, \tilde{\mathbf{x}}_i) - \eta(\mathbf{x}, \tilde{\mathbf{x}}_j))^2}{\left(\sum_i p(\mathbf{x}|\tilde{\mathbf{x}}_i)\right)^2}, \tag{S19}$$

which is strictly positive in any direction. □

C Experimental Details

In all our experiments, we largely follow the experimental setup and evaluation protocol of [58], with some differences due to our novel approach and hardware limitations, which we describe below. Both α and $\tilde{\alpha}$ are parameterized by separate three-layer neural networks with dimensions 20, 20, and 1. The second layer has an additional skip connection and we use GELUs [22] as hidden activation. We normalize both networks to a mean of zero over a batch and use an additional learnable bias c .

Our model is optimized using Adam [32] with a base learning rate of 10^{-4} for the encoder and c . For α and $\tilde{\alpha}$ we use a learning rate of 10^{-2} .

We train all models for 3×10^5 iterations, except for 3DIdent, where we train for 1×10^5 iterations, and the experiments in Section 4.5 when $n > 10$, where we set the number of iterations to 8×10^5 .

We use the same encoder architecture and batch size as in [58] on KITTI Masks (64) and 3DIdent (512). However, for the experiments in sections 4.1, 4.2 and 4.5, we use a smaller neural network with residual connections and a smaller batch size of 5120 when $n \leq 10$ and 4096 when $n > 10$. The residual network has 2 hidden layers with $n \cdot 10$ and $n \cdot 20$ dimensions followed by 3 residual blocks and the output layer. Each residual block has 2 layers with $n \cdot 20$ dimensions each. In all hidden layers we use leaky ReLU activations and batch normalization.

The experiments in Section 4.1 and Section 4.2 ran on a GeForce GTX 1080 Ti GPU for between 7 and 30 hours, depending on the space configuration, shape parameter, and loss function. The experiments on KITTI Masks took on average 2 hours on a GeForce GTX 1080 Ti GPU and the experiments on 3DIdent took on average 24 hours on four GeForce GTX 1080 Ti GPUs.

Table S1: Identifiability on synthetic data. R^2 [%] mean \pm standard deviation over 2 random seeds

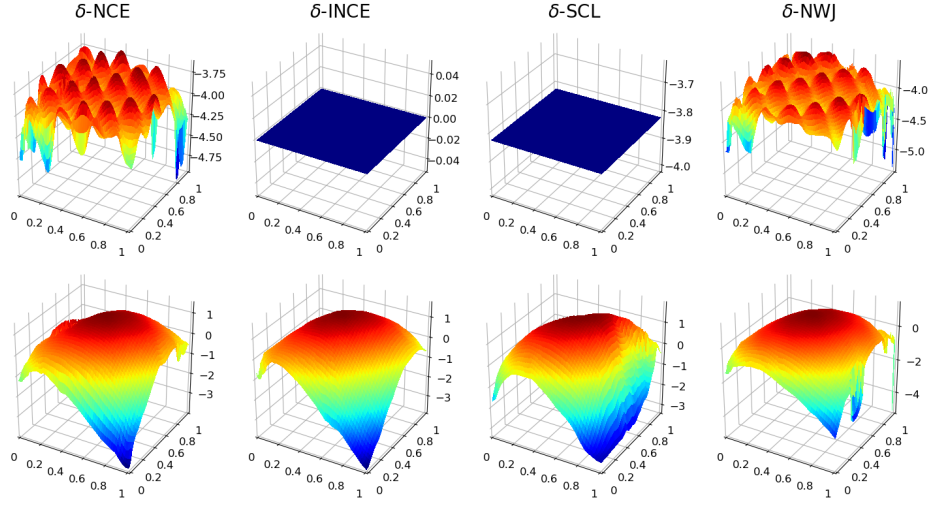
Scenario	β	δ -NCE	δ -INCE	δ -SCL	δ -NWJ
Box (simple)	1/2	99.48 \pm 0.03	99.26 \pm 0.35	86.38 \pm 2.55	99.71 \pm 0.03
Box (simple)	1	99.89 \pm 0.01	99.88 \pm 0.01	92.80 \pm 1.03	99.83 \pm 0.04
Box (simple)	3	99.68 \pm 0.17	94.49 \pm 4.90	97.21 \pm 0.14	99.65 \pm 0.11
Box (simple)	5	99.74 \pm 0.06	94.31 \pm 4.66	97.85 \pm 0.59	99.73 \pm 0.02
Box (complex)	1	98.72 \pm 0.54	99.80 \pm 0.09	91.51 \pm 1.25	97.17 \pm 2.75
Box (complex)	3	99.87 \pm 0.01	99.76 \pm 0.01	97.37 \pm 0.18	99.79 \pm 0.04
Hollow ball	1	99.54 \pm 0.21	99.51 \pm 0.13	87.88 \pm 6.63	99.56 \pm 0.14
Hollow ball	3	95.39 \pm 4.34	96.78 \pm 0.03	96.05 \pm 0.09	98.41 \pm 0.15
Hollow ball	5	97.61 \pm 0.33	94.08 \pm 0.87	95.98 \pm 0.16	97.90 \pm 0.29
Cube grid	1	99.82 \pm 0.03	99.54 \pm 0.03	95.67 \pm 2.37	99.72 \pm 0.01
Cube grid	5	96.80 \pm 0.09	88.74 \pm 1.03	94.65 \pm 0.06	97.83 \pm 0.01

Table S2: R^2 [%] scores on synthetic data for $\alpha = \tilde{\alpha} = c$

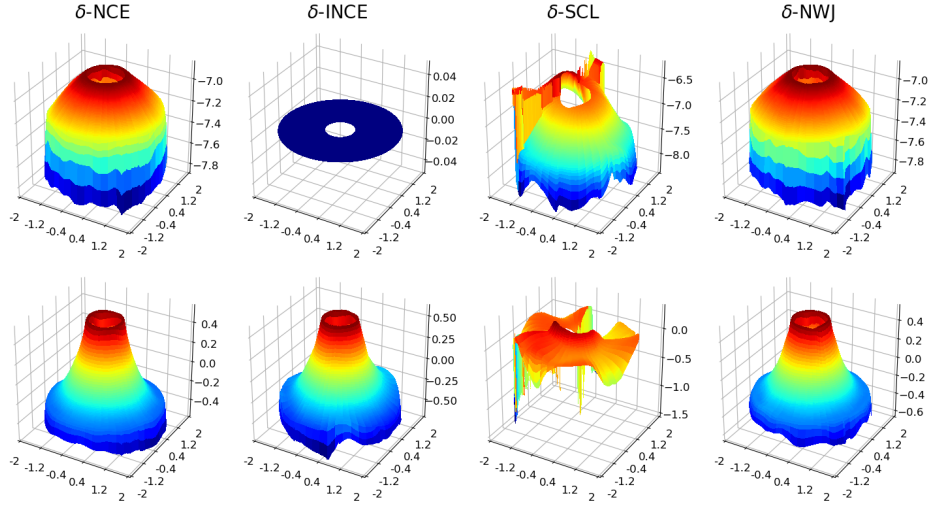
Scenario	β	δ -NCE	δ -INCE	δ -SCL	δ -NWJ
Box (simple)	1/2	99.21	99.69	86.83	88.30
Box (simple)	1	99.77	99.91	92.85	99.70
Box (simple)	3	99.61	99.31	99.65	99.59
Box (simple)	5	99.84	99.13	94.15	99.83
Box (complex)	1	99.54	99.71	85.08	99.45
Box (complex)	3	99.46	99.70	91.79	99.10
Hollow ball	1	97.13	98.91	79.50	96.06
Hollow ball	3	97.55	95.64	94.21	97.69
Hollow ball	5	97.19	93.77	97.11	97.18
Cube grid	1	99.75	99.14	97.20	99.62
Cube grid	5	95.88	83.73	97.20	97.41

D Additional Experiments

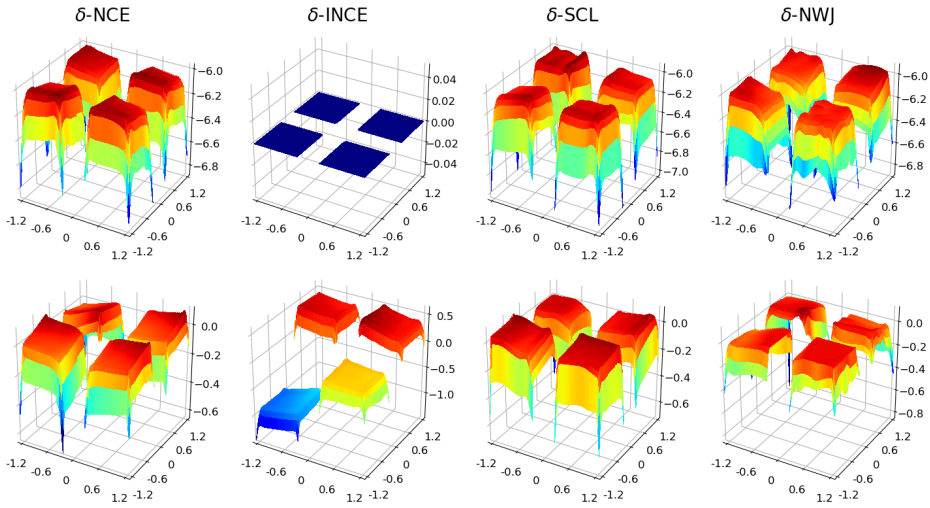
Table S1 and Table S2 contain the corresponding R^2 values for the experiments in Section 4.1 and Section 4.2, respectively. Figure S1 shows the learned functions α and $\tilde{\alpha}$ for the three configurations *box (complex)*, *hollow ball* and *cube grid*. Furthermore, Table S3 shows R^2 and MCC values for the original SCL [20] loss.



(a) Box (complex)



(b) Hollow ball



(c) Cube grid

Figure S1: Learned functions $\alpha \circ h$ (top rows) and $\tilde{\alpha} \circ h$ (bottom rows) for configurations (a) box (complex), (b) hollow ball and (c) cube grid. In the case of δ -INCE, α is set to zero.

Table S3: Identifiability on synthetic data for the original SCL [20]. R^2 and MCC [%] mean \pm standard deviation over 2 random seeds

Scenario	β	R^2	MCC
Box (simple)	1/2	94.46 \pm 2.94	55.52 \pm 4.63
Box (simple)	1	89.06 \pm 0.09	57.38 \pm 0.89
Box (simple)	3	88.80 \pm 0.08	57.05 \pm 1.62
Box (simple)	5	89.84 \pm 0.71	55.51 \pm 2.19
Box (complex)	1	91.12 \pm 0.07	56.02 \pm 0.83
Box (complex)	3	91.02 \pm 0.06	51.45 \pm 3.14
Hollow ball	1	84.69 \pm 1.81	52.97 \pm 2.08
Hollow ball	3	22.59 \pm 1.11	22.16 \pm 1.24
Hollow ball	5	19.97 \pm 1.31	23.46 \pm 1.22
Cube grid	1	43.88 \pm 4.91	32.45 \pm 4.24
Cube grid	5	20.09 \pm 1.64	23.53 \pm 2.19